

ELEVENTH EUROPEAN ROTORCRAFT FORUM

Paper No. 54

FURTHER STUDIES OF HELICOPTER ROTOR ICE ACCRETION AND PROTECTION

R. W. Gent
R. H. Markiewicz
J. T. Cansdale

ROYAL AIRCRAFT ESTABLISHMENT, FARNBOROUGH, ENGLAND

September 10-13, 1985
London, England.

THE CITY UNIVERSITY, LONDON, EC1V OHB, ENGLAND.

FURTHER STUDIES OF HELICOPTER ROTOR ICE ACCRETION AND PROTECTION

by

R. W. Gent
R. H. Markiewicz
J. T. Cansdale

Royal Aircraft Establishment, Farnborough, England.

ABSTRACT

Recent research at RAE into icing on helicopter rotors is reviewed. Mathematical models have been developed to predict accretion of ice on rotor blades and of the thermal behaviour of electrothermal rotor deicing protection systems. The accretion model predicts ice formation on a rotor for both the hover and forward flight cases. Comparisons are presented between wind tunnel and flight accretion measurements and corresponding model predictions, and some preliminary assessment is made of the effects of forward flight on ice accretion. Both 1- and 2-dimensional models of electrothermally deiced rotors have been developed and results are shown to illustrate their capabilities. Overall assessments are made of the models' limitations and their applicability to system design and certification.

Results are also presented from an experimental study of the relative sensitivity of a NACA 0012 and an RAE cambered section aerofoil to aerodynamic degradation by ice, represented by a simple geometric spoiler. Significant differences were found in the effects on the lift, pitching moment and stall characteristics of the two sections.

1 INTRODUCTION

The capability for flight in icing conditions is a continuing high priority requirement for current and future helicopters, both military and civil. At present, several types of helicopter have clearances to fly in a limited range of icing conditions without the safeguard of a rotor protection system, whilst a few now have electrothermal rotor deicing systems and are achieving more extensive clearances.

Although in the past the certifications have been based primarily on the evidence of flight in natural cloud, the problems and limitations of this have long been realised. In particular, icing flight trials are very expensive and are dependent on nature to provide suitable weather. Although the aim is to clear the helicopter to extreme conditions, these will by definition occur very rarely, and some compromise has to be reached in terms of the level of experience which is acceptable as a basis for clearance.

In recent years, much thought and effort has been given to the contribution which other techniques, such as the use of prediction methods and simulation, may make to design, development and certification, so as to reduce the duration of natural icing trials. Whilst it must be accepted that some natural testing will always be necessary, the use of other methods to interpolate and extrapolate flight results to the extremes of the atmosphere and performance envelopes will be a major benefit.

The current paper describes two aspects of the recent work in RAE concerned with rotor icing, and records the progress since the previous Forum paper in

1980 (Ref 1). Firstly, mathematical models have been developed to predict the accretion of ice on rotor aerofoils (in terms of extent, shape and growth rate) and to predict the thermal behaviour of electrothermal deicing systems; in discussing these, attention is given to their acceptability for the particular applications for which they may be intended. Secondly, wind tunnel experiments have been conducted to investigate the relative sensitivity of the traditional NACA 0012 aerofoil and a modern cambered section to degradation by ice. Both these aspects make important contributions towards the understanding and prediction of rotor performance in icing.

2 MATHEMATICAL MODELLING

2.1 Application

In developing and assessing the mathematical modelling it is important to consider the tasks to which they may be applied. Although these will obviously vary between the individual analyses, three broad applications may be identified:

- a. Understanding the observed behaviour of helicopters in icing, of either natural or simulated (e.g Ottawa Icing Spray Rig) origin.
- b. Design, particularly of protection systems.
- c. Direct application to the certification process, for instance for interpolation or extrapolation of flight test results.

The model's ability to meet these conditions is reviewed at the end of each section.

2.2 Ice accretion prediction

2.2.1 General description of the model

The aim is to predict the shape, extent and rate of ice growth at any given spanwise station of the rotor. The problem is simplified to either steady (hover) or quasi-steady (forward flight) 2-Dimensional flow and without wake interaction effects. Furthermore, the predictions are made for a clean aerofoil, and as such the ice growth rates predicted should be regarded as initial ice growth rates, since the resulting ice layer will change both the aerodynamics and the water catch characteristics of the aerofoil. However, research has shown that there is considerable scope for this single time step technique which is proving adequate for the relatively small accretions likely to be associated with a deiced aerofoil.

As in previous studies of ice accretion, such as that by Messinger (Ref 2), the RAE model is based on the assumption that the icing of a surface is governed by the balance of a number of heat flows, eg kinetic heating, convective cooling, evaporative cooling, latent heat of freezing and so forth. The RAE model, however, represents a significant step forward in that a full allowance is made for compressible flow effects. The kinetic heating and convective cooling terms are combined such that the ambient air temperature in the classical equation for convection, is replaced by the adiabatic boundary layer recovery temperature, itself a function of local static pressure. A new evaporative cooling term has also been developed to take account of the variation in water vapour concentration at the edge of the boundary layer due to

the variation in local pressure. This means that for instance in the upper surface suction region where the air is expanded and cooled, the water vapour concentration is reduced, resulting in further heat loss by evaporation in this region. Full details of the heat balance equations may be found in Ref 3.

In practice, the heat balance equations are applied to a number of small zones, equally spaced along the aerofoil surface. The local icing condition in each zone is found by evaluating the heat balance, which determines the local surface water freezing fraction, n_f , and subsequently enables the surface temperature and ice growth rate to be calculated. The freezing fraction dictates the type of ice formed. White, opaque rime type ice forms when all the impinging water freezes on impact ($n_f=1$). Conversely, translucent, glaze ice forms when only part of the impinging water freezes ($0 < n_f < 1$). Any unfrozen water is included in the heat balance for the next downstream zone.

An ice shape prediction is made from the local growth rates by extrapolation to a given time. The direction in which the growth rates are applied to the aerofoil surface has received much attention in the past. For single time step models, it is now becoming widely accepted that the growth rates are applied normal to the aerofoil surface for glaze type accretions and in a direction parallel to the main airflow direction (usually taken as the aerofoil incidence) for rime accretions; the latter method produces a more realistic rime ice shape, and allows predictions to be made at larger time steps.

The latest RAE model combines three separate accretion models into one extremely versatile aerofoil accretion prediction package. The three models cover:

- 1) Accretion in hover (fixed airspeed and incidence) assuming no heat conduction within the blade structure,
- 2) Accretion in hover as above, but with heat conduction in the blade, and
- 3) Accretion in forward flight (cyclic variation of both incidence and airspeed) with heat conduction in the blade.

The first two models are used to predict initial values (zero azimuth position) for the blade temperature and ice growth rate distributions used in part three of the package. This reduces the computer time needed to find the forward flight solution, and also provides a reference solution to quantify the effects of the cyclic parameters on the accretion.

The layout and input data for the models are summarised in Fig 1. The atmospheric and rotor details are relatively straight forward. The main inputs to the models are chordwise distributions for clean surface pressure ratio, P/H , convective heat transfer coefficient, h_c and surface water droplet catch efficiency, β ; the latter being the local fraction of the free stream liquid water concentration (LWC) impacting the aerofoil surface. The pressure ratio data base is generated using the RAE Garabedian and Korn program (Ref 4). The chordwise pressure distribution is stored for a range of Mach number and incidence values (typically $M=0.1-0.7$ in 0.1 intervals and $\alpha=0^\circ-12^\circ$ in 1° intervals) and the desired pressure distribution is obtained by interpolation.

Convective heat transfer coefficients are difficult to calculate and the problem has only recently been overcome after considerable research. Even now, an empirical approach has had to be adopted and it is likely to be some time before a purely theoretical method is developed. The present method approximates the leading edge of the aerofoil to a cylinder and uses the generalised form of the distribution for heat transfer from the surface of a roughened cylinder (Ref 5). Experimental measurements in the USA (Refs 6,7) have confirmed the basic form of this distribution.

The size of the cylinder and the coefficients in the generalised heat transfer distribution are found by matching a theoretical prediction for a glaze ice shape with an experimental, tunnel or flight ice shape. The empirical relationships are based on the cylinder Reynolds number, and research has shown that the scaling properties of this variable can be utilised, allowing the heat transfer coefficient distributions to be calculated for a wide range of atmospheric and flight conditions.

Finally, the water catch distribution is calculated from a set of generalised curves which are written in terms of the modified inertia parameter, K_0 (Ref 8) and aerofoil incidence. Only certain key variables, such as peak value catch efficiency, and limits of water droplet impact are generalised. Interpolation is used to obtain the local water catch efficiency at each surface zone. Crucial to this generalised catch efficiency approach is the need to calculate the water droplet catch distribution on an arbitrarily shaped aerofoil for a range of K_0 and aerofoil incidence. At RAE we have developed such a program, which is described below.

2.2.2 Droplet trajectory calculations

Due to the complex nature of the airflow about rotor systems, it is necessary to make the simplifying assumptions that steady two dimensional compressible flow calculations are acceptable, and that wake interaction effects have negligible influence on the ice accretion process. Experimental evidence to date, suggests that these assumptions are acceptable.

The trajectory of a super-cooled water droplet about an arbitrary shaped aerofoil is found by integrating the governing equations of motion of the droplet. The governing equations, expressed in non-dimensional form, have been formed in the standard way by assuming that aerodynamic drag is the only force affecting the particle motion; the drag law proposed by Langmuir and Blodgett (Ref 9) has been used.

In the equations of motion there is a non-dimensional grouping of terms called the inertia parameter, K , which relates airspeed, droplet diameter and aerofoil chord. A large value of K produces high values of local catch efficiency, and implies large water droplets travelling at high speed and impacting on a small chord aerofoil. Whilst K may be used for scaling analyses, a better parameter is the so called modified inertia parameter, K_0 , which is formed from the product of the inertia parameter and a correction term relating aerodynamic drag to Stoke's law drag. This produces a parameter which is better for scaling in airspeed.

The integration requires the airflow to be known or calculable at every position the droplet may occupy. For the RAE trajectory model, the Viscous Garabedian and Korn (VGK) (Ref 4) program, developed by Aerodynamics Department RAE for transonic flow predictions, is run to provide a data file containing velocity component data for the required Mach number/incidence case.

Interpolation by the trajectory program within these data provides the desired values of the local airstream velocity components.

Integration is performed using a fourth order Runge-Kutta numerical integration process with the integration step length reduced automatically as the droplet nears the aerofoil surface. This maintains the accuracy of the integration whilst using a minimum number of integration steps.

The local surface water catch efficiency is found by calculating two trajectories which have a small separation in the free stream. The separation between the initial trajectories divided by the separation between impact points on the aerofoil surface is a measure of the surface water catch.

Outputs from the model are the surface distribution of water catch, which includes the limits of water droplet impact, and a value for the overall catch efficiency, E , which is the ratio of the volume of intercepted water to the geometric swept volume of the aerofoil.

Validation of the model against experimental results is extremely difficult since it is impossible to produce a suitable cloud of single sized droplets. Also, the high turbulence levels in icing tunnels, caused by the the water spray mast, has an unknown effect on the droplet trajectories. An alternative approach to validation is by comparison with results from other theoretical studies on droplet trajectories (Refs 9-11). The simplest test is to compare results for catch efficiency on a cylinder under incompressible flow conditions, with the data published in Ref 9. Additional confidence is obtained now that other researchers have made similar comparisons (Refs 10,11). The RAE model showed excellent agreement with all the published data (Ref 12), which shows the mathematical aspects of the program to be correct.

More appropriate are comparisons for water catch on aerofoils. Under a NASA/MOD(PE) agreement on helicopter icing a number of test case trajectory calculations have been compared to further validate the respective models, and also quantify the effects of air compressibility on catch efficiency distribution. Comparisons covered the incidence range 0° to 8° and Mach numbers from 0.175 to 0.8 on a symmetric NACA 0012, and non-symmetric Wortmann FX-69-H-098 aerofoil at two values of inertia parameter, K . The K values were chosen to give high and low extremes of water catch appropriate to helicopter rotors. The results showed excellent agreement for the high K values ($K=0.72 - 3.0$) over the complete range of Mach numbers. Fig 2 illustrates this agreement for the high K case (with $K=3.0$) at $M=0.8$. Slight differences in catch distribution were found however, for the low K values at Mach numbers above $M=0.4$ ($K= 0.12 - 0.24$). Fig 3 shows the relatively small differences in predicted catch distribution obtained with $M=0.8$ and $\alpha=0^\circ$.

Fig 4 summarises the magnitude of compressibility effects on the overall catch efficiency for the Wortmann aerofoil at zero incidence. Plotted is the percentage difference in E relative to the value at $M=0.175$, for a range of K_0 values. There appears to be a threshold Mach number above which compressibility effects are present, and which leads to a slight reduction in catch efficiency (and catch limits). Note that the magnitude of the compressibility effects varies with K_0 . In terms of the non-dimensional parameter, Q , (Ref 9) (which combines the droplet Reynolds number and the inertia parameter K) the threshold value is in the range $1.3-1.5 \times 10^5$.

2.2.3 Applications and limitations

The present model addresses impingement only. It is assumed that the intersection of a trajectory with the surface implies the droplet will attach. Experimental observations suggest that this may not be true for highly oblique impacts on aerofoils, such as at the limit of water droplet impact. Thus the model is probably acceptable for producing the input to the accretion model, where the leading edge is the main consideration, but may give an overestimate of catch limits, especially on the aerofoil lower surface, and may therefore be more limited in its usefulness for heated rotor blade system design, where there is a need to calculate the surface area to be protected by heating elements. A programme of experimental work on the impact of small water droplets at highly oblique angles under representative conditions is planned for the near future.

The effects of 3-D flow and turbulence are unknown, as is the effect of the rotor inflow on the cloud. For forward flight, with cyclic variation of velocity and incidence, the assumption that instantaneous catch is governed by instantaneous flow is probably acceptable. Notwithstanding these comments the model is probably acceptable for quantifying the likely differences in water droplet catch between different rotor systems and different cloud conditions (e.g effect of larger droplets, or benefits from a larger chord rotor).

The velocity gradient across the boundary layer is not included in the trajectory calculation, though its effect on a trajectory would probably only be significant in the region of the catch limits. Calculations with a viscous correction to the inviscid flowfield have shown negligible differences in predicted catch for aerofoils at incidence.

2.3 Ice accretion in hover without blade heat conduction

To a first order approximation any spanwise station of the rotor is assumed to have a fixed aerofoil incidence and Mach number. The problem is then identical to icing on a fixed wing aircraft, with steady, 2-dimensional, compressible flow. Without heat conduction the heat balance equations are mathematically independent (apart from the runback water term) and the equations can be solved in a step-by-step process starting at the airflow stagnation point. The equilibrium icing surface temperature is found using the Newton-Raphson technique, using a polynomial function for the ice/water vapour pressures (Ref 13)

Fig 5 shows comparisons between theoretical and experimental (icing tunnel) ice shapes formed on a 30 cm chord, NACA 0012, fully composite, aerofoil over a range of icing conditions. Initially, the heat transfer coefficient distribution was optimised to give agreement between experiment and theory for case 5.1/b. From this distribution, the equation coefficients are derived which are used subsequently in the model subroutine for the calculation of heat transfer coefficient at all Mach numbers and incidences. The level of agreement is remarkable considering the single time step approach used, and indicates the method is acceptable at least for accretions with a maximum size of 2% x/c .

In Fig 6 the same heat transfer equation constants have been used for predictions on a US Army UH-1H helicopter flown in the NRC Canada, Ottawa Icing Spray Rig (Ref 14). The agreement is good for accretions on inboard stations but there is an overprediction of ice shape outboard of approximately 60% span. The reasons for this are not yet understood but possible explanations include the droplet bounce phenomenon mentioned above, centrifugal effects and low LWC

towards the edge of the spray cloud. Note that the test conditions for the cloud and for rotor incidences contain a large degree of uncertainty. The agreement shown was obtained using a much warmer static air temperature than quoted (-14 instead of -19°C). The only explanation for this is that the air temperature was measured out of the cloud and that steam atomising nozzles are used to produce the droplet cloud, which might conceivably raise the air temperature of the fairly localised cloud.

A notable feature of the new heat balance equations is the ability to predict the so called beak ice accretions (Ref 1), which form in the upper surface suction region of the aerofoil under relatively warm conditions. The local reduction in pressure in this region produces local cooling which is sufficient to freeze out part of the warm runback water. Observations in rig experiments indicate that the size of the accretion is self limiting, with the consequent loss of lift causing an increase in local surface pressure and hence temperature to a point at which no further ice grows. On a rotor, beak ice accretions will grow outboard of the normal spanwise limit of leading edge/lower surface ice, and can extend close to the tip even at temperatures above -5°C . Due to the strong influence of suction on its formation, the extent of beak ice will probably be affected by collective pitch, itself a function of aircraft all-up-weight and flight condition. It may also be very transient in nature, with a small reduction in aerofoil incidence causing the ice to shed. Fig 7 shows an example of beak ice accretion formed during rig experiments at a total temperature of $+4.7^{\circ}\text{C}$, a Mach number of 0.4, and incidence of 8° . The corresponding model prediction is given in Fig 8, which shows the position of the accretion to be in agreement with the experimental result.

2.4 Ice accretion in hover with blade heat conduction

The assumption of a non-conducting structure is unrealistic for almost all practical blade constructions. Even blades made of composite construction, which have low thermal conductivity, usually have metal erosion shields which provide a conductive path. Part 2 of the model considers a 2-dimensional blade geometry in which the construction is represented by a number of finite width, parallel, flat plates. Spanwise heat conduction may be ignored because the temperature gradients in this direction are small, even towards the blade tip. The heat balance equations are now inter-dependent and must be solved using a slightly more complex method. A Gauss-Siedel underrelaxation technique has been successfully employed, which uses the results from the non-conducting rotor model as the initial estimates for zonal (nodal) temperatures and surface freezing fractions. The number of iterations required to obtain a converged solution depends upon the thermal conductivities in the layer construction and upon the ice type. With a glaze ice shape it is necessary to relax values of the freezing fraction at certain nodes instead of the temperature. This affects the downstream runback water terms, which consequently slows convergence.

Results from the conduction model (Fig 9) show significant effects for a bare alloy construction, whilst an all composite construction behaves virtually as a non-conductor. However, considering more typical constructions, an alloy construction protected with a polyurethane erosion tape, has very similar icing characteristics to a composite structure protected by a metal erosion shield.

The conditions under which heat conduction is likely to have most effect on the icing characteristics of a rotor are at the thresholds for icing and for rime/glaze ice type. Results for the latter constructions described above have shown little difference in icing characteristics at these threshold conditions. Rig observations using a test specimen with half metal, half composite

construction have confirmed the theoretical predictions (see Fig 7).

It should be noted that there is no allowance for heat conduction within the predicted ice layer, which would provide an extra conductive path. From the limited number of comparisons with experimental data, this omission seems acceptable at present.

2.5 Ice accretion in forward flight

In forward flight, any given spanwise station will experience cyclic changes in both incidence (pitch) and velocity. The former will increase the primary catch area of the aerofoil, and will also produce a cyclic variation of pressure and hence temperature in the suction region. Cyclic velocity will cause variations of temperature and other parameters over the whole blade surface. How the rotor surface temperature responds to these transient effects will be determined by the thermal properties of the various layers in the blade construction. A blade made from thermally insulating material is likely to confine any temperature variation to a region close to the rotor surface, and a rotor with a high specific heat content material (i.e a material with a high density x specific heat product) will tend to reduce the magnitude of the cyclic effects, whilst also introducing a phase difference between the driving external heating and the response of the blade surface.

The aim of the forward flight model is to find the equilibrium conditions for the azimuthal variation of temperature and surface growth rate. The ice growth rates are averaged over a complete revolution which allows an ice shape prediction to be made as for the hover case models. The model uses a 2-dimensional, transient, finite difference scheme to solve the equations, with the blade structure represented by a series of flat plate layers. Typically 12% chord, top and bottom surface is modelled with insulated edge boundary conditions assumed at the chordwise limits. A converged solution is reached in about 8 revolutions when using 100 steps in azimuth.

At present the incidence variation is sinusoidal, with representative values determined from rotor load prediction programs assuming a Glauert downwash model (Ref 15).

Figure 10, compares the response of a typical composite and metal blade rotor under wet and warm (non-icing) conditions. Shown is the azimuthal variation in surface temperature at the 1% surface distance to chord point on the aerofoil upper surface. The metal erosion shield in the composite construction dissipates the cyclic heating remarkably effectively, whilst the polyurethane erosion tape on the metal spar blade shows approximately 1° variation with azimuth and with an approximately 45° phase shift between the peak heating (at 90° azimuth) and peak temperature response of the blade.

It is likely that the effects of forward flight will be most evident at the threshold icing conditions. Figs 11 and 12 compare the predicted hover and forward flight threshold conditions for icing in the suction region (beak ice threshold) and stagnation line respectively, on a Wessex helicopter. The forward airspeed was taken at 80 Kts, with an AUW of 6350Kg and 5000ft altitude. Also, the hover results are for the lower altitude of 500ft. Three curves are shown for the beak ice threshold; icing threshold using the static Mach number/incidence equivalent to the mean incidence/Mach number of forward flight, the threshold with cyclic varying incidence/Mach number and the threshold for hover. The cyclic effects produce a shift in the threshold relative to the meaned values equivalent to about 1°C in outside air temperature (OAT). The

higher air density at the lower altitude used for the hover case, results in lower aerofoil incidences and less peak suction on the upper surface. Hence a colder OAT is needed to produce icing. In this particular case there is little difference between the thresholds for forward flight and hover. It is also interesting to note that the forward flight beak icing threshold represents a balance between melting on the advancing side of the disc and freezing on the retreating side.

The stagnation line icing threshold is independent of aerofoil incidence (Fig 12). 80Kts forward flight produces a drop in threshold OAT of between 1 and 2 °C depending on radial position. Also shown in Fig 12 are results from the analysis of inflight tail boom camera photographs, which recorded the spanwise extent of icing on the lower surface of a Wessex rotor for a number of natural icing flights. The comparison between flight and theory is remarkably good.

The validation of the model has still to be completed. This has been severely delayed by the lack of experimental ice shapes with which to make the necessary comparisons. The model has been checked for mathematical errors and is now considered to give an accurate solution to the problem as modelled. Fig 13 shows a comparison between theory and experiment for rime and glaze ice shapes formed in an icing tunnel with the aerofoil oscillated in pitch. The rime ice shape is satisfactory but the glaze ice shape only manages to predict the characteristic rounded horns. This is probably due to the simplistic approach taken for the convective heat transfer coefficient which, at present, is centred on the air stagnation point and moves with it as the incidence changes.

2.6 Applications and limitations

The model is acceptable for comparing the relative effects of atmospheric and rotor parameters in terms of the ice shape produced. It is probably also acceptable for providing input conditions to the modelling of heated rotor blade systems. However, before the model can really be used in the certification process, the minimum detail necessary to allow an acceptable performance degradation assessment to be made (either by subsequent wind tunnel-flight trial measurements using replica ice, or purely theoretical means) must be established. Further comparisons with ice shapes formed on helicopter rotors, rather than in icing wind tunnels, are considered necessary to complete the validation of the model.

3 TEMPERATURE TRANSIENTS CALCULATIONS

3.1 General

The incorporation of electrical heating elements (typically five) into the leading edge of a helicopter rotor, is now well accepted as the most viable means of preventing excessive ice build up. In operation, individual elements are heated according to a given sequence and heat on-time in order to raise the rotor-ice interface temperature above 0°C. When a number of elements have been energised, achieving melting over a sufficiently wide surface area, a combination of aerodynamic and dynamic forces is able to complete the shedding process. A new ice layer is then allowed to grow before the heating sequence is repeated.

One and two dimensional explicit, finite difference models have been written to predict the temperature history of points within an electrothermally

deiced rotor from a given set of starting conditions. The rotor construction is represented by a series of parallel flat plate layers, with heat input at a specified layer interface.

3.2 1-D Model

Model development started with a program having a convective heat transfer boundary at the internal (hollow D spar) and external (ice-air) surfaces. Heat input is switched off after a specified time to model structural temperatures on cool-down, and any ice layer present is 'shed' after the blade-ice interface has exceeded 0°C for an arbitrary period of time (typically 0.5 sec.). The concepts of this early model are described in Ref 16 and are based on the work by Stallabrass (Ref 17).

Subsequent refinements now include the ability to: set the initial temperature of the structure to that of the equilibrium iced surface value, calculated using the heat balance approach described above; model the melting-refreezing of the ice using a simple moving interface technique; allow for the correct heat transfer from the external surface by evaluating the appropriate icing heat balance.

In the latest model the ice layer will be shed if any of the following conditions are met

- (1) the water layer exceeds a preset maximum thickness,
- (2) the ice layer reduces to less than a preset thickness,
- (3) a specified number of heating cycles has been completed.

Note that an ice layer will not be modelled if the unheated equilibrium icing surface temperature is predicted to be above the freezing point. The model will also predict the formation of a new ice layer after the old has been shed. This feature is particularly useful for studying non-optimised deicing systems in which heat is applied before sufficient ice has grown and, which can result in excessive amounts of runback water being generated.

Fig 14 shows a comparison between theory and laboratory experiment for a 1-D heating case with ice phase change. Plotted is the temperature history for the blade - ice interface. Note the change in slope when the ice melts.

Fig 15 shows results from a typical deicing run with the rotor surface temperature and ice / water thicknesses plotted as a function of time. Criteria 1 (water layer greater than 0.5mm) and 3 (end of heating cycle two) have been used to shed the ice and water layers.

To date, the model has been mainly used as a basic design tool. This includes a preliminary investigation of the maximum temperatures reached by glue and spar layers in composite blade constructions. Fig 16 shows an example of the program output for a spar temperature prediction run in which the failure case of no ice shedding is considered. This might occur if the flanks of the accretion were improperly heated, either due to an inadequate heating sequence or to a failure of the aft heating elements. Note that with the ice unremoved the spar temperature continues to rise. The height of the temperature peak has been found to be strongly related to the thickness of base coat material between the heating element and the main spar structure.

3.3 2-D Model

The development of a 2-dimensional model is still at a relatively unrefined level, though once again it is useful for basic design studies.

The edgewise limits of the model are represented by insulated/symmetric boundary conditions and convective heat transfer boundaries are again employed for the internal and external surfaces. Any size or combination of elements and element insulation gaps can be modelled, although the ice layer thickness and surface boundary conditions remain constant for all element and gap sections.

A recent refinement has been the inclusion of ice phase change modelling using the equivalent specific heat method. This program has now been validated against other numerical solutions for problems with 1-D symmetry.

Fig 17 shows blade-ice interface temperature distributions, for a small chordwise section of rotor blade, at 2 second intervals from heat on. The case considers the energisation of a single heating element of width 20mm (symmetry has been assumed and hence only half the element is modelled), in which heat is lost by chordwise conduction into a 10mm width of unheated section. An insulated boundary condition is applied to the right hand edge of the section, which approximates to a free conducting boundary, for this case, since the heater has a negligible effect on the structure temperatures in this region.

At the end of the 10 second heating period only 70% of the heater width has achieved melting, indicating the significant heat sink an adjacent area poses. The temperatures above the centreline area of the heater are also sufficiently uniform for a 1-D model approximation to be made.

Future refinements will include a more accurate, moving interface phase change routine which will use conformal transformation techniques to model more realistically shaped ice layers having non-uniform thickness. The modelling of the heat transfer from the iced surface will also be improved using the heat balance approach.

At present only isotropic properties are modelled. For composites, particularly those with carbon fibre, it will be necessary to allow for anisotropic thermal conductivity.

Future work will be aimed at validating the model by comparing predictions with both icing tunnel and flight results. Experience so far suggests that the accuracy of the model is limited not so much by the mathematics as by the quality of the input data. It is essential, though sometimes difficult, to have accurate values for layer thicknesses and material thermal properties.

3.4 Applications and limitations

The main limitation with both models, which restricts their use to design exercises at present, is the fact that the ice shedding criteria from a rotor in flight are not well known. It is unlikely that melting over the complete blade-ice interface is necessary to achieve shedding in practice, since the aerodynamic and dynamic loading on the ice is likely to assist the process. A 1-D model is unlikely to ever model the ice shedding process accurately, although empirical criteria, based on either surface temperature or water layer thickness, may give a conservative approximation.

Other limitations, which are perhaps more easily overcome, are the fact that the 2-D model is incapable at present of modelling the non-uniform ice layer thickness found in practice, and is unable to model the formation of runback water, acknowledged as an unavoidable consequence of a thermal type deicing system. The modelling of runback water is however likely to be a lesser problem since it is intended to use good design to minimise its formation. The main application of the models at present is therefore in the basic design of heated rotor blade systems, in which prohibitively high internal temperatures can be avoided and selection of a heater blanket and additional covering layers with the best thermal properties made.

4 AEROFOIL PERFORMANCE DEGRADATION

4.1 Introduction

As a first step towards understanding the relative sensitivity of different aerofoils to ice accretion, comparative experiments have been carried out using simple geometric spoilers. The two aerofoils used were NACA 0012, a traditional section, and an RAE cambered section which is representative of modern sections designed to achieve higher lift coefficients at the high incidence/low Mach number conditions appropriate to helicopter rotors.

The icing simulation consisted of a reproducible protruberance on the upper surface of the aerofoil (see Fig 18). A metal strip 0.25 mm wide and either 0.2 or 0.5% chord high, was positioned in a channel running parallel to the leading edge, and which in turn could be located at five chordwise stations: 0, 2, 5, 15 and 30% chord. (No boundary layer trip was used). The leading edge positions at 0, 2 and 5% chord were chosen to investigate the effects of the initial build up of ice (including beak ice), whilst the aft chordwise positions were chosen to investigate the effect of refrozen runback water generated during deicing. Each aerofoil was equipped with eighteen pressure transducers on the upper surface and twelve on the lower surface, for calculating the lift and pitching moment coefficients. The tests were carried out in the ARA, 0.2m x 0.46m, 2-D blowdown wind tunnel using the pitch and heave rig with 0.1m chord blades. Tests covered Mach numbers from 0.3 to 0.6 in quasi-steady, oscillatory and ramp (constant rate) pitch conditions.

4.2 Parameters considered

In this paper, test results are examined for conditions that correspond to two regions of the rotor disc that are of particular interest in cruising flight. The first region is the fore and aft sector which generates most of the rotor lift. Here, the blade Mach number lies between 0.4 and 0.6, with C_L typically in the region of 0.6. Any loss in lift due to ice accretion must be compensated for by an increase in collective pitch, which will then drive the retreating blade closer to its stalling incidence. Blade stall in the tip region of the retreating blade has severe consequences and this region of the disc is the second one to be considered. Here, blade Mach number is typically between 0.3 and 0.4 and C_L approaching $C_{L_{max}}$.

4.3 Results

When examining test results for the first set of conditions, it is convenient, because of differences in zero-lift angle for the two aerofoils, to present data in the form of loss of C_N for a given value of C_N for the 'clean' aerofoil, as in Fig 19. For this case the protruberance was positioned at 2% chord and a 1500 deg/sec pitch rate used, which for the reduced model scale

represents conditions at the front of the disc.

Remembering that the cambered aerofoil would be expected to be operating at a somewhat higher value of C_N than NACA 0012, we see both aerofoils suffer a similar loss in C_N (about 0.05) in their operating range. The same conclusion was drawn from the test results for different protruberance positions close to the leading edge.

The first assessment of the effects of the protruberance at low Mach number and high angles of attack has been made by considering the fractional loss in the maximum value of the normal force coefficient. Fig 20 shows this loss plotted against the chordwise position of the protruberance. The results show that NACA 0012 is most sensitive to the strip positioned between 0 and 2% chord, whereas the corresponding region is between 2 and 5% chord for the RAE section. Also, the RAE section was degraded more than NACA 0012 for positions aft of 5% chord.

By plotting the pitching moment coefficient against the blade incidence, the incidence at pitching moment break (α_{CMB}) can be determined, which has been defined as the angle corresponding to a drop in pitching moment coefficient of 0.01 relative to the zero lift value. The effect of the protruberance on the fractional loss of α_{CMB} is shown in Fig 21 for the 1500 deg/sec ramp motion. The results are very similar to those described above.

4.4 Performance degradation conclusions

The results of the tests indicate that there is little difference in the sensitivity of the two aerofoils, to the initial accretion of ice, over the front of the disc at their expected operating conditions. However, in terms of the effect of the initial ice accretion on the retreating blade, we see that the greatest loss in C_{Lmax} occurs for a different position of the protruberance for the two aerofoils. Furthermore, the cambered aerofoil is seen to be more sensitive to the protruberance well back from the leading-edge, suggesting a greater sensitivity to runback ice. This type of information is of considerable value in deciding on deicer mat positions and the heating sequence.

The exercise has been a very good first attempt at assessing the likely performance implications of icing. However, future work should use more representative ice shapes. Since the potential range of ice shapes is infinite some compromise on what constitutes a representative shape has to be made, and the work recommended in section 2.6 on establishing the minimum detail for acceptable performance assessment will undoubtedly be of great benefit to this exercise.

5 Overall conclusions

5.1 Considerable progress has been made in the development of theoretical models for predicting the icing and deicing of helicopter rotor blades. Specifically:

(1) The water droplet trajectory and hover case ice accretion models have been demonstrated to predict both rime and glaze ice shapes to a reasonable accuracy, and can now find application, such as in the interpretation of flight observations and for parametric studies.

(2) Ice shapes predicted by the forward flight ice accretion model show a general agreement with the limited number of experimental shapes available.

Further comparisons are needed, particularly with flight data, for cases where the velocity is varying cyclically. A small difference between the icing thresholds in hover and forward flight has been predicted.

(3) The electrothermal deicing models are providing important insights into the functioning of deicing systems, and are already being applied to design problems. However, some refinements and further validation against experimental and particularly flight data is considered necessary if they are to be used in the certification process.

5.4 The tunnel tests on aerofoil sections degraded by a protruberance intended to represent ice were extremely useful in assessing the likely sensitivity to icing. Future work should however consider more representative ice shapes.

5.3 The work is considered to be an essential step towards the prediction of the performance of both unprotected and protected rotors in icing.

List of symbols

c	Aerofoil chord (m)
E	Overall catch efficiency (%)
h_c	Convective heat transfer coefficient ($W.m^{-2}.K^{-1}$)
K	Droplet inertia parameter, (non-dimensional)
	$K = \rho V D^2 / 18 \mu c$ $V = \text{free stream velocity (m/s)}$ $D = \text{water droplet diameter (m)}$ $\mu = \text{air viscosity (N.s/m}^2\text{)}$ $\rho = \text{droplet density (kg/m}^3\text{)}$
K_o	Modified inertia parameter, (non-dimensional)
	$K_o = K \lambda / \lambda_s$ $\lambda_s = \text{Stoke's law droplet range (m)}$ $\lambda = \text{Actual droplet range in air (m)}$
LWC	Cloud liquid water concentration (g/m^3)
M	Mach number (-)
n_f	surface water freezing fraction (-)
OAT	Static air temperature ($^{\circ}C$)
p_{∞}	air pressure (kPa)
P/H_o	surface local pressure ratio (-)
R	Blade radius (m)
s/c	Surface distance to chord ratio (-)
x/c	chordwise position (-)

- Z protruberance height (-)
- α aerofoil incidence ($^{\circ}$)
- β local surface water catch efficiency (%)
- α Dimensionless variable,
- $$\alpha = 18 \rho_a^2 Vc / \mu \rho \quad \rho_a = \text{air density (kg/m}^3\text{)}$$

References

- 1 Cansdale, J.T., Helicopter rotor ice accretion and protection research. Sixth European Rotorcraft Forum, Bristol, September 1980.
- 2 Messinger, B.L., Equilibrium surface temperature of an unheated icing surface as a function of airspeed. J. Aeronautical Sciences 20,1,29-41, 1953.
- 3 Cansdale, J.T. and Gent, R.W., Ice accretion on aerofoils in 2-Dimensional compressible flow - A theoretical model. RAE TR82128, Jan 1983.
- 4 Collyer, M.R., An extension of the method of Garabedian and Korn for the calculation of flow past an aerofoil to include the effects of a boundary layer and wake. RAE TR 77104, July 1977.
- 5 Achenbach, E., The effects of surface roughness on the heat transfer from a circular cylinder to the cross flow of air. Int. J. Heat and Mass Transfer 20, 359-369, 1977.
- 6 Fossen, G.J.V., Simoneous, R.J., et al, Heat transfer distributions around nominal ice accretion shapes formed on a cylinder in the NASA Lewis icing research tunnel. AIAA-84-0017, 1984.
- 7 Arimilli, R.V., Keshock, E.G., et al, Measurements of local heat transfer coefficients on ice accretion shapes. AIAA-84-0018, 1984.
- 8 Bowden, D.T., Gensemer, A.E.C., and Skeen, C.A., Engineering summary of airframe icing technical data. General Dynamics/Convair, San Diego CA, technical report ADS-4. Also contract report FA-WA-4250 for FAA, Dec 1963.
- 9 Langmuir, I. and Blodgett, K. B., A mathematical investigation of water droplet trajectories. Army Air Forces TR no. 5418, 1946
- 10 Bragg, M.B., Rime ice accretion and its effect on airfoil performance. NASA contract report 165599, March 1982.
- 11 Lozowski, E.P. and Oleskiw, M.M., Computer simulation of airfoil icing without runback. AIAA paper no. 81-0402, 19th Aerospace sciences meeting, St Louis, Missouri, Jan 12-15 1981.
- 12 Gent, R.W., Calculation of water droplet trajectories about an aerofoil in steady, 2-Dimensional, compressible flow. RAE TR 84060, 1984.
- 13 Lowe, P.R., An approximate polynomial for the computation of saturation

vapour pressure. J. Applied Meteorology 16, pp100-103, Jan 1977.

- 14 Shaw, R.J., Richter, P. The UH-1H helicopter icing flight test program: An overview. Paper No. AIAA-85-0338 presented at the 23rd Aerospace Sciences meeting, Reno, Nevada, USA, JAN 14-17, 1985.
- 15 Young, C., A user's guide to some computer programs for predicting helicopter and rotor performance. RAE Unpublished work.
- 16 Gent, R.W., Cansdale, J.T., 1-Dimensional treatment of thermal transients in electrically deiced helicopter rotor blades. RAE TR 80159, Dec 1980.
- 17 Stallabrass, J.R., Thermal aspects of deicer design. Paper presented at the International Helicopter icing conference, Ottawa May 1972.

Copyright ©, Controller HMSO London, 1985.

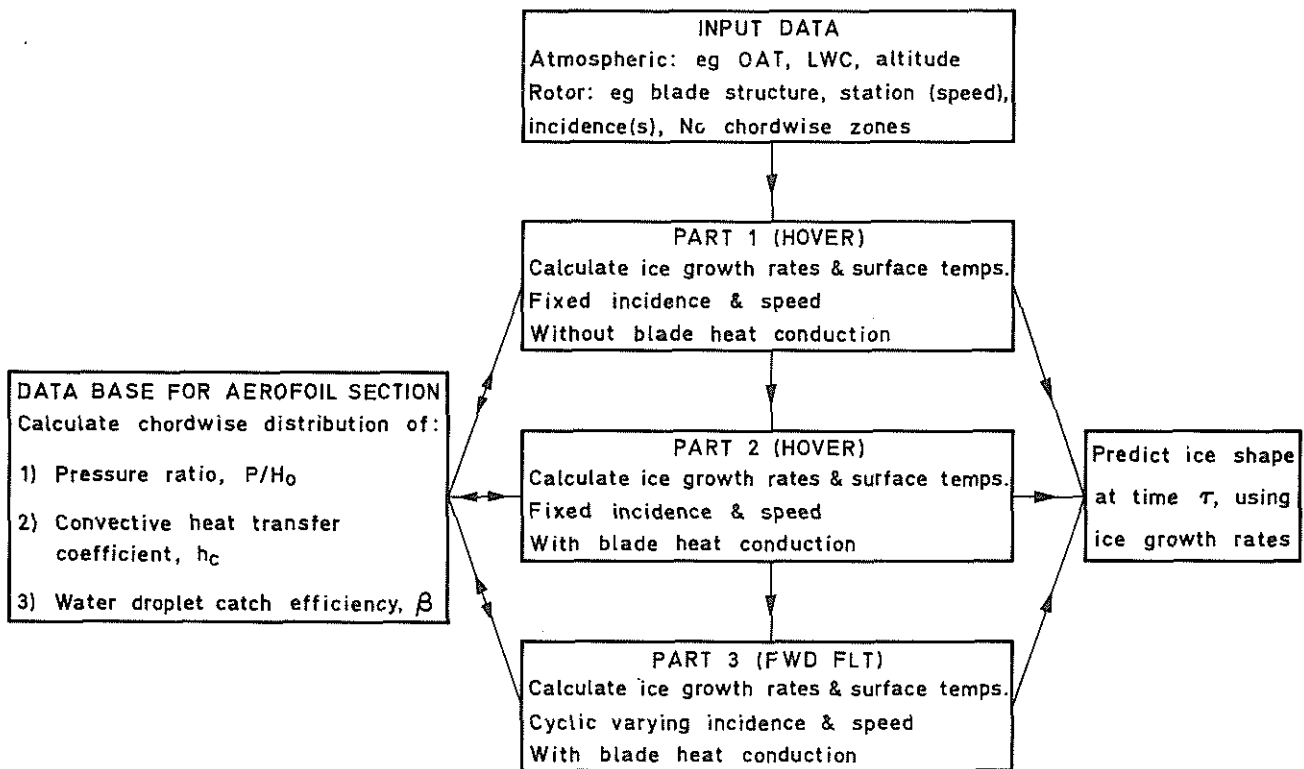


Fig 1 Block diagram of RAE ice accretion program

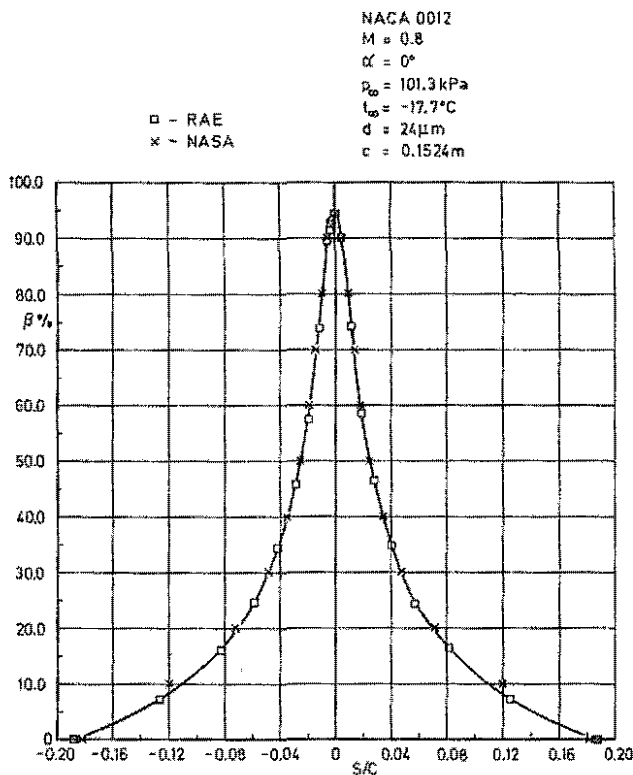


Fig 2 Comparison of RAE and NASA results for water droplet catch efficiency on a NACA 0012 aerofoil; high K value (3.0)

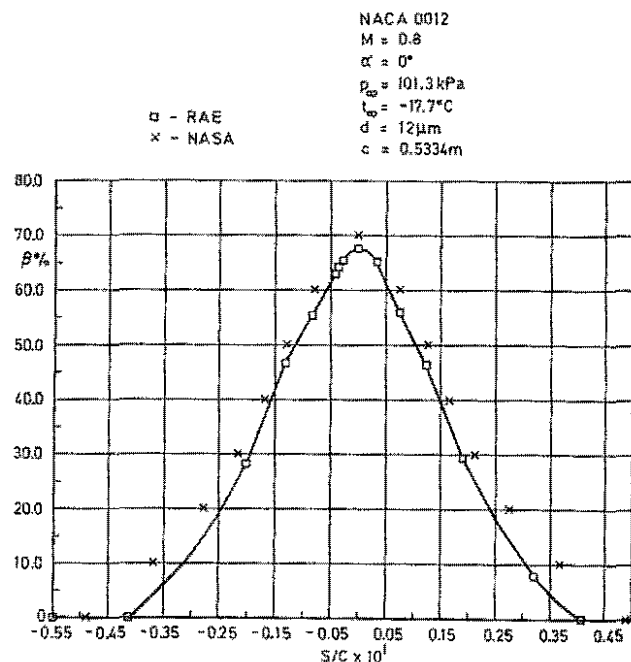


Fig 3 Comparison of RAE and NASA results for water droplet catch efficiency on a NACA 0012 aerofoil; low K value (0.24)

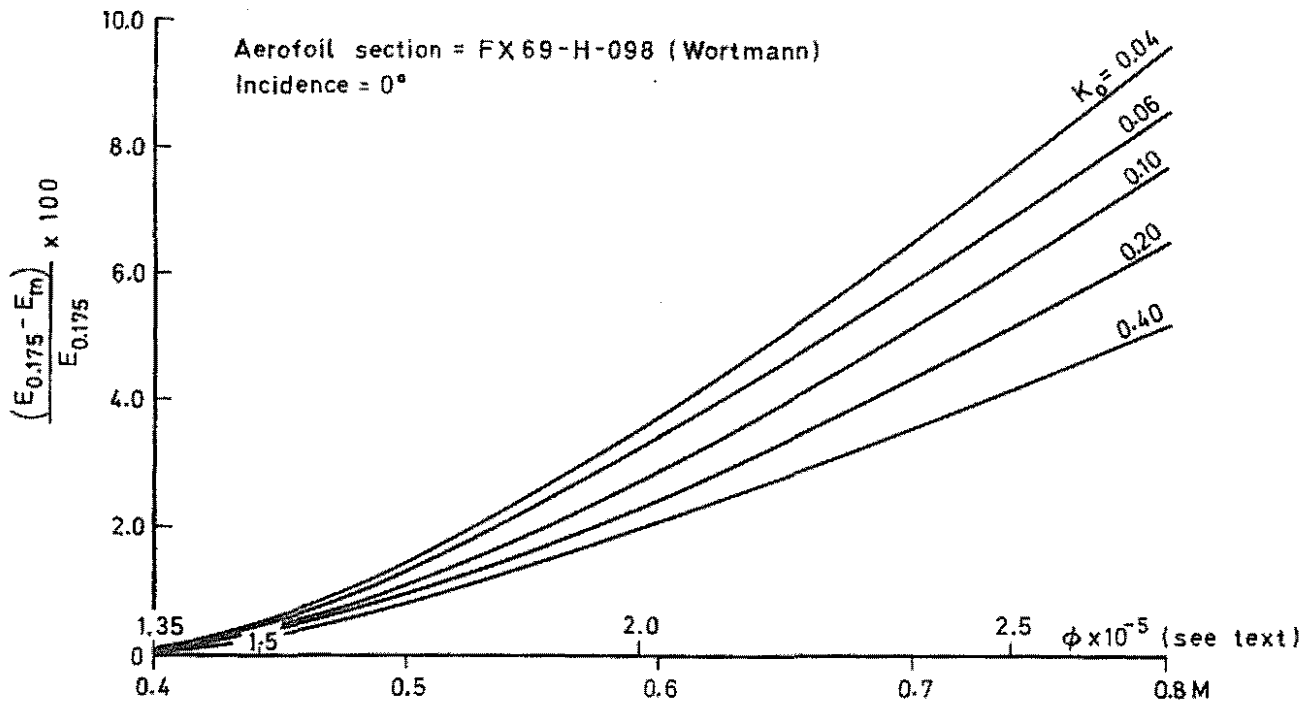


Fig 4 Effect of air compressibility on overall catch efficiency, expressed as a percentage difference relative to the value at $M = 0.175$

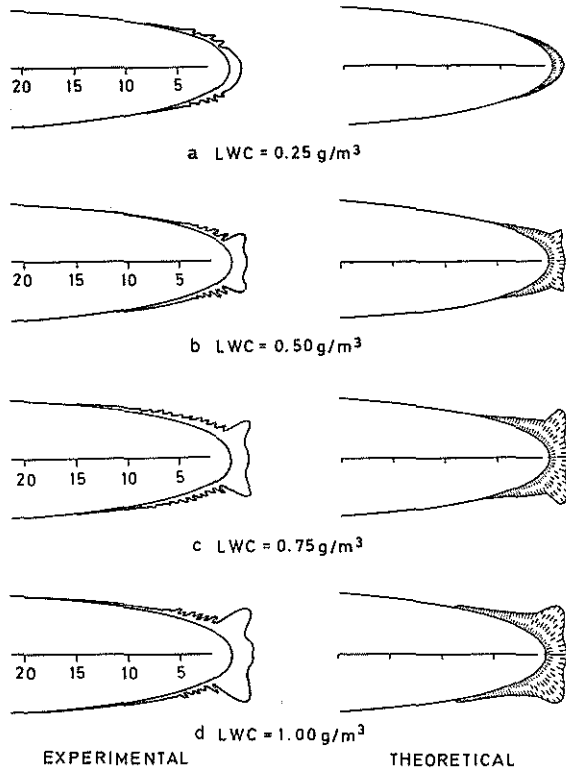


Fig 5.1 The effect of LWC on ice shape, with $\alpha = 0^\circ$, $M = 0.4$, $OAT = -12.6^\circ\text{C}$ and Time = 2 min

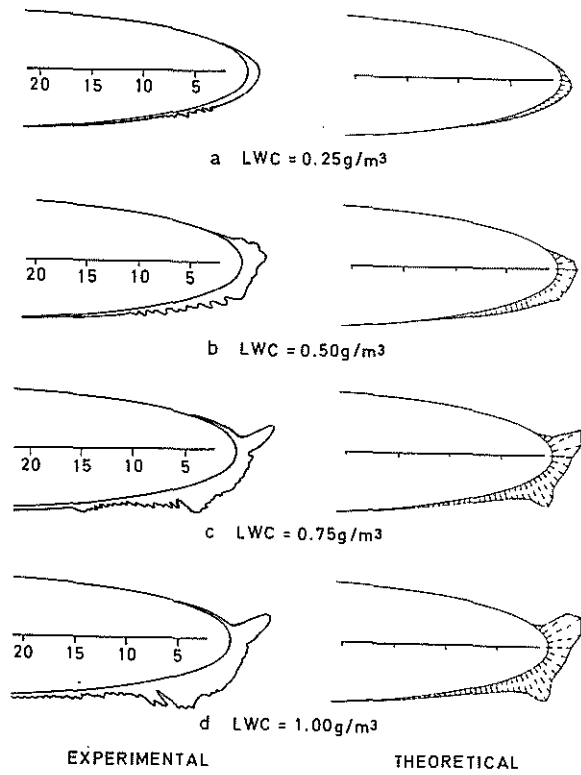


Fig 5.2 The effect of LWC on ice shape, with $\alpha = 4^\circ$, $M = 0.4$, $OAT = -12.6^\circ\text{C}$ and Time = 2 min

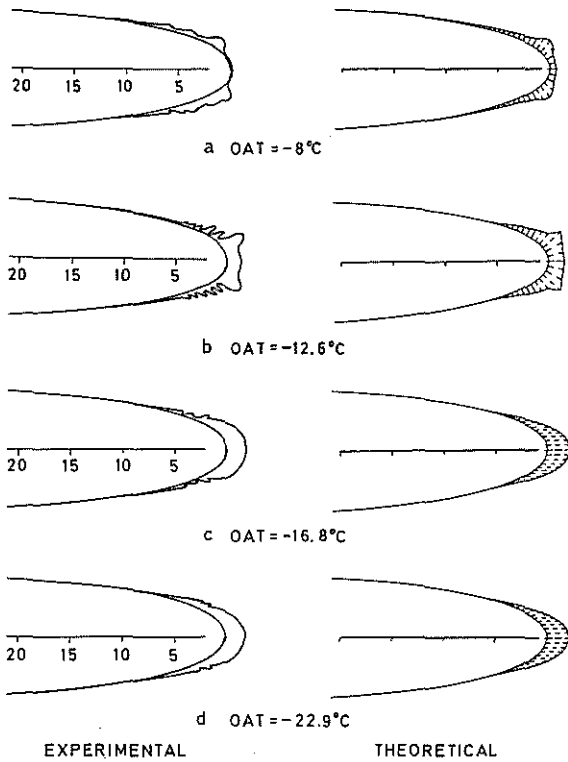


Fig 5.3 The effect of OAT on ice shape with $\alpha = 0^\circ$, $M = 0.4$, $LWC = 0.5 \text{ g/m}^3$ and Time = 2 min

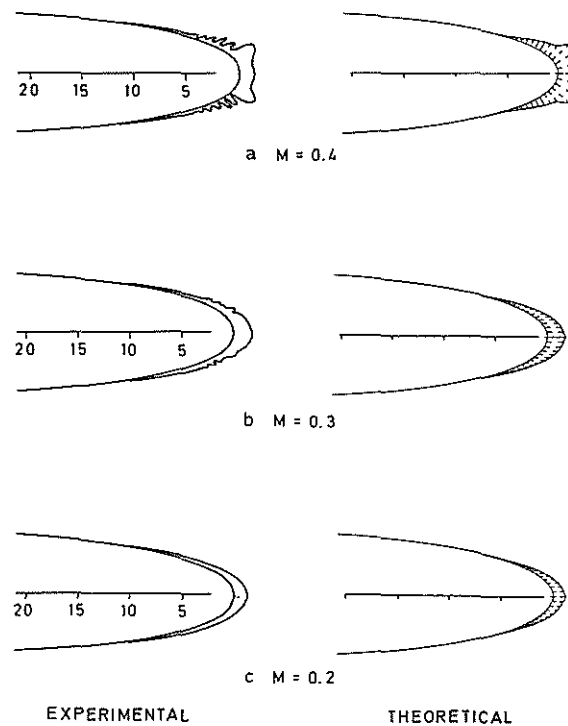


Fig 5.4 The effect of Mach number on ice shape with $\alpha = 0^\circ$, $OAT = -12.6^\circ\text{C}$, $LWC = 0.5 \text{ g/m}^3$ and Time = 2 min

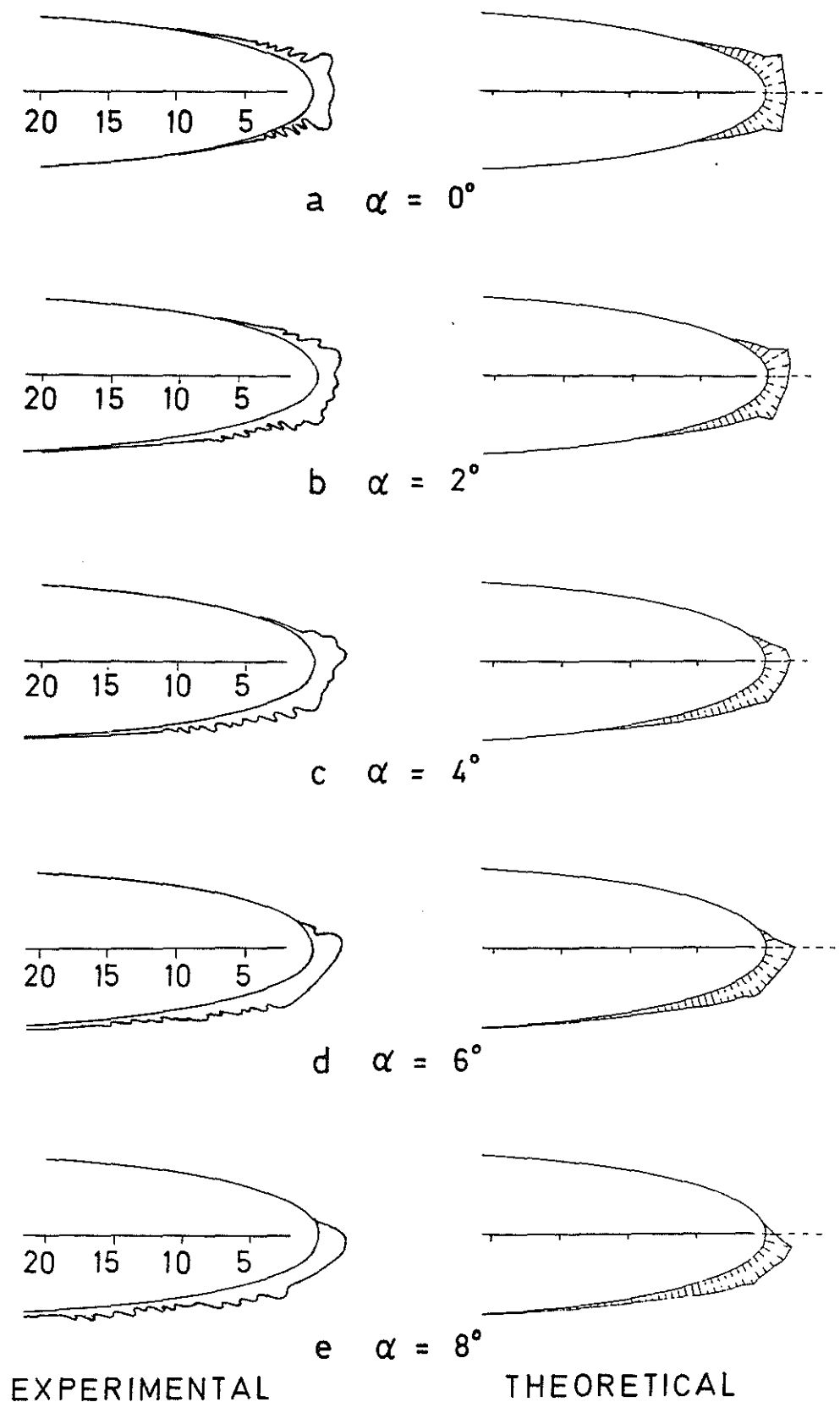


Fig 5.5 The effect of incidence on ice shape with $M = 0.4$, $OAT = -12.6^\circ\text{C}$, $LWC = 0.5 \text{ g/m}^3$ and Time = 2 min

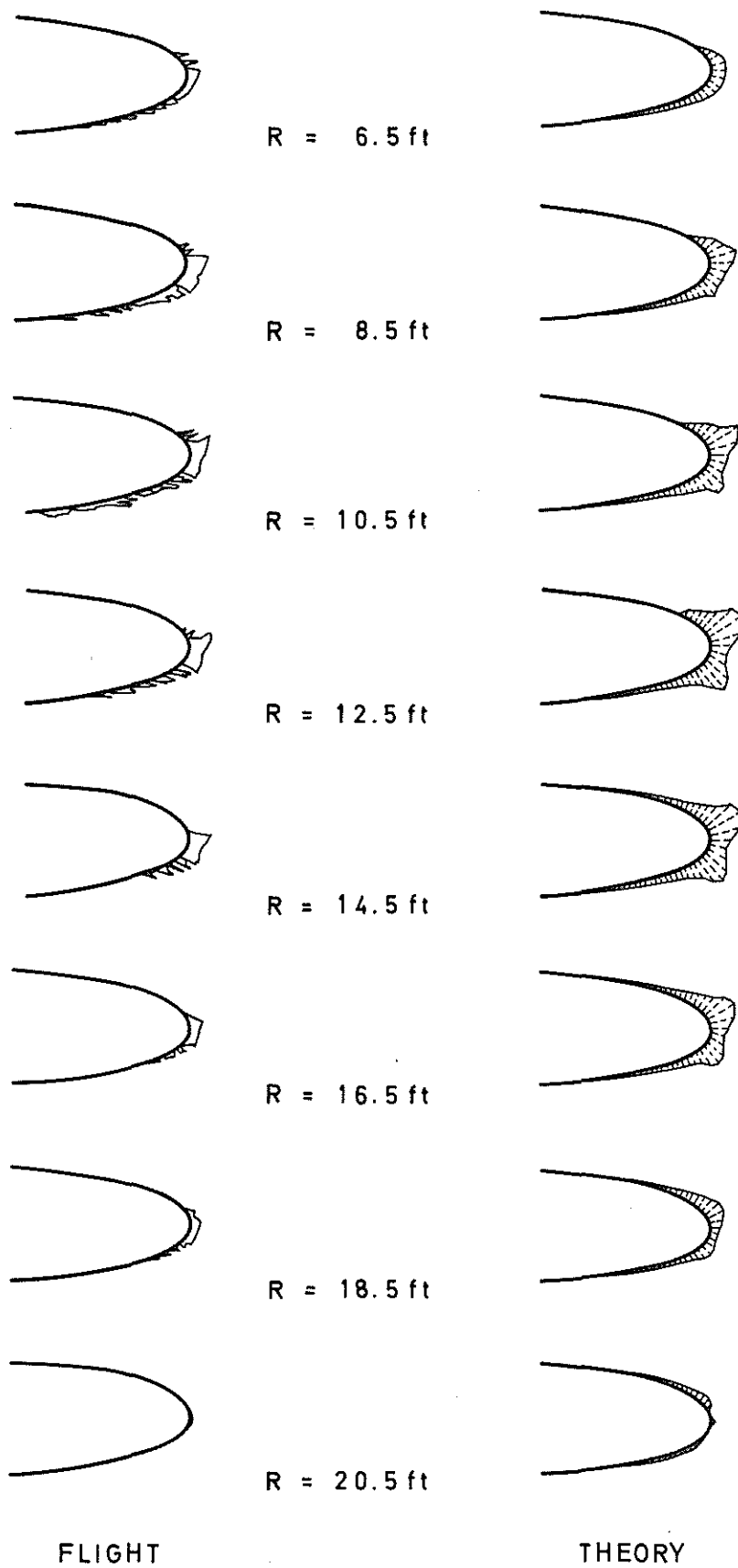


Fig 6 Comparison of flight ice shapes with theory prediction. The helicopter was a US Army UH-1H, flown in the NRC icing spray rig, Ottawa

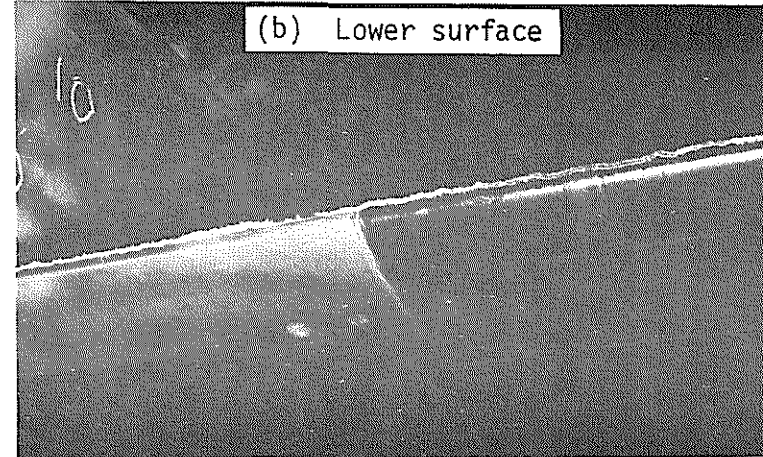
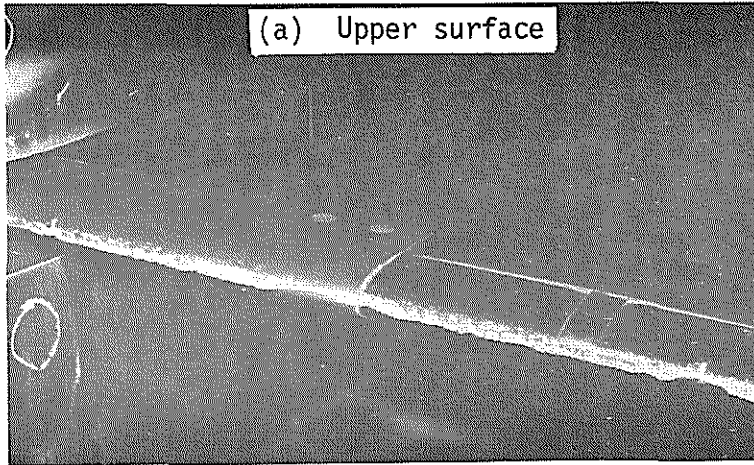


Fig 7 Example of beak ice growth. Aerofoil has half metal, half composite spar construction. $t_T = +4.7^\circ$, $M_\infty = 0.4$, $LWC = 0.6 \text{ g/m}^3$, $c = 0.465 \text{ m}$, $\alpha = 8^\circ$, time = 2.5 minutes

54-21

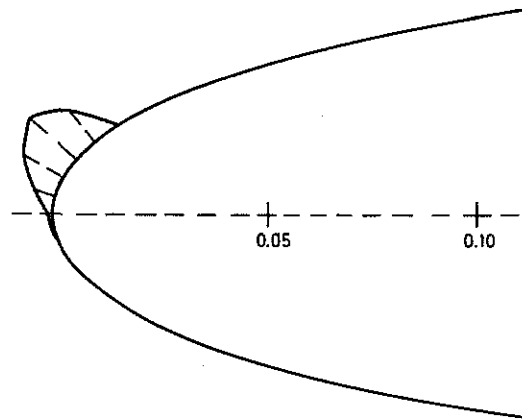


Fig 8 Theoretical prediction of beak ice growth corresponding to the tunnel ice shape of Fig 7

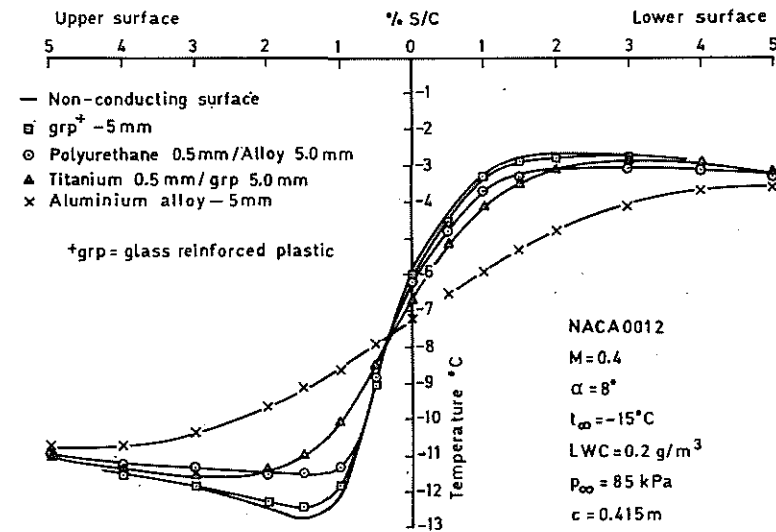


Fig 9 Effects of blade heat conduction on surface temperature

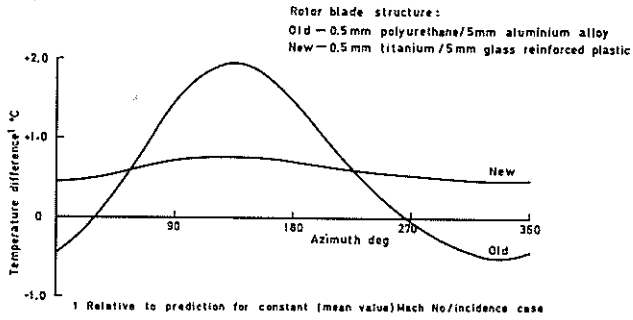


Fig 10 Surface temperature response of a typical old and new generation rotor blade to the effects of cyclic varying Mach number and incidence in helicopter forward flight. Position = 1% s/c upper surface, span = 0.7 R, $V_{TIP} = 205$ m/s, advance ratio = 0.2, $\alpha = 5.7^\circ \pm 3^\circ$

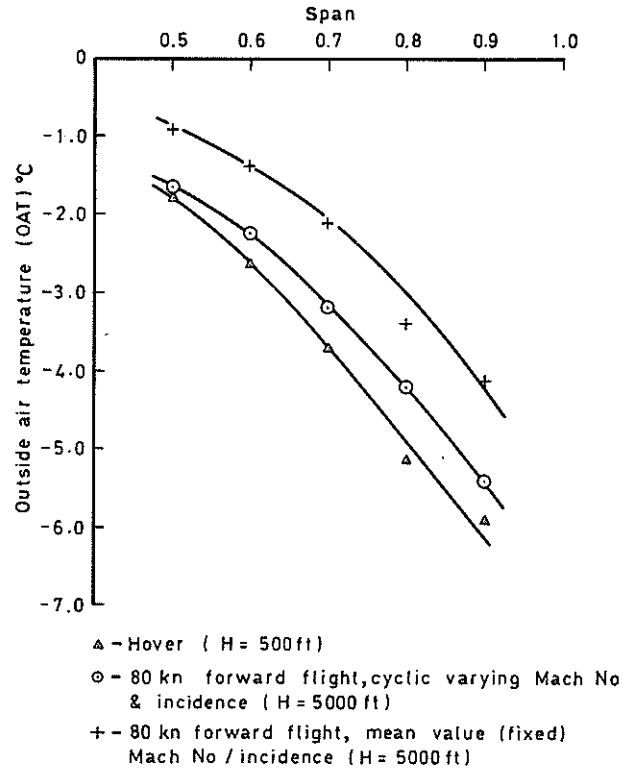


Fig 11 Upper surface beak icing threshold as a function of rotor span and flight condition

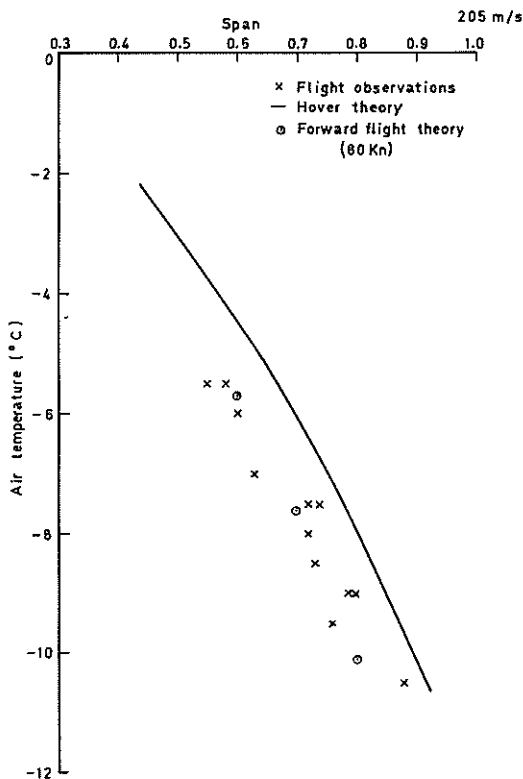


Fig 12 Stagnation line icing threshold as a function of rotor span

$M = 0.4$ - constant $\alpha = 4^\circ \pm 4^\circ$ (3.8 Hz)
 $c = 0.68$ m $p_\infty = 69.5$ kPa
 Time = 5 minutes

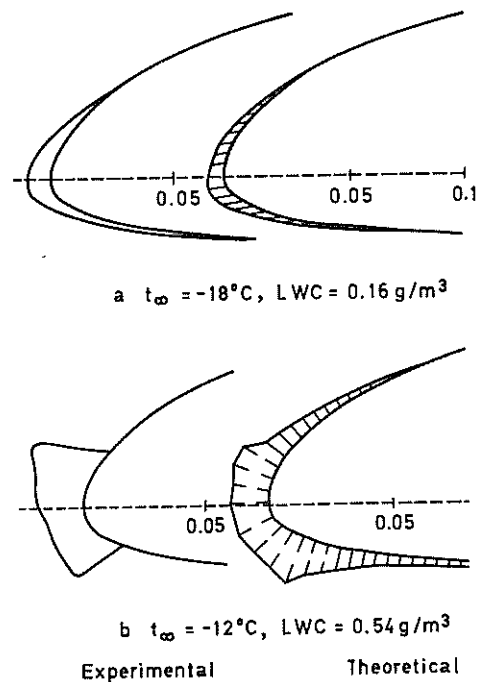


Fig 13 Comparisons between experiment and theory for the 'cyclic' accretion model

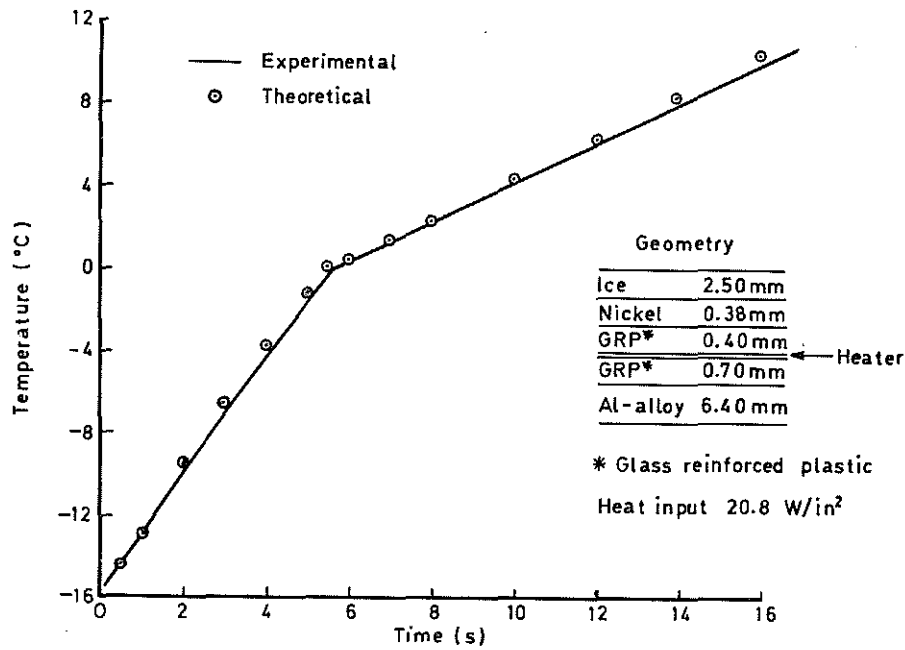


Fig 14 Comparison between experimental and theoretical temperature response of a heated slab. Temperature shown is for the Nickel-Ice interface

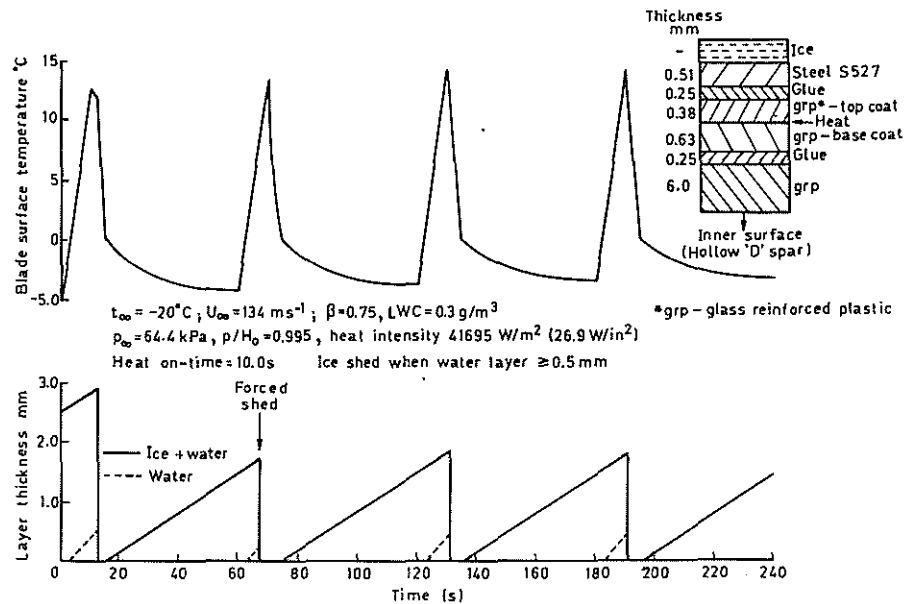


Fig 15 Typical 1-D deicing model results

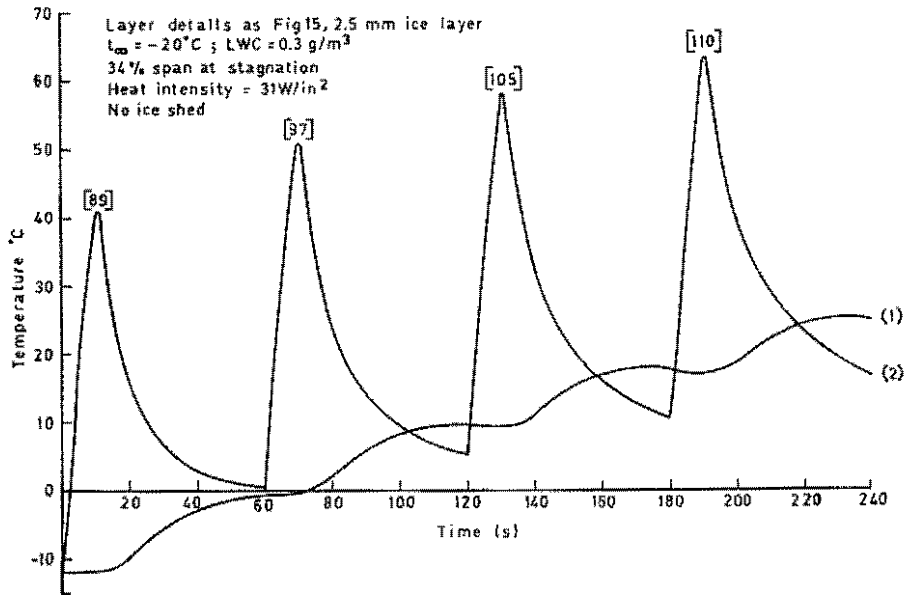


Fig 16 Spar temperature predictions for the blade inner surface (1) and below the base coat glue line (2). The peak heating element temperature is shown in square brackets

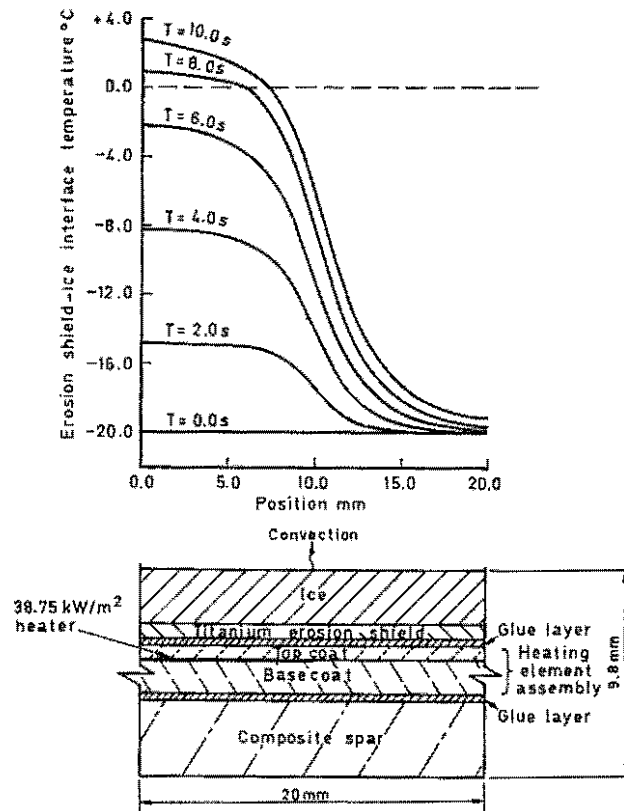


Fig 17 Example results from the 2-D heated rotor blade model

$Z = 0.2\%$ or 0.5% chord
 $X = 0, 2, 5, 15$ or 30% chord

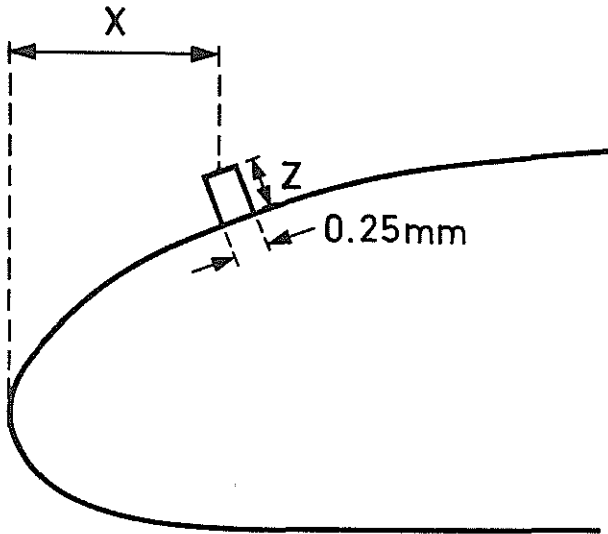


Fig 18 Protruberance mounted on aerofoil

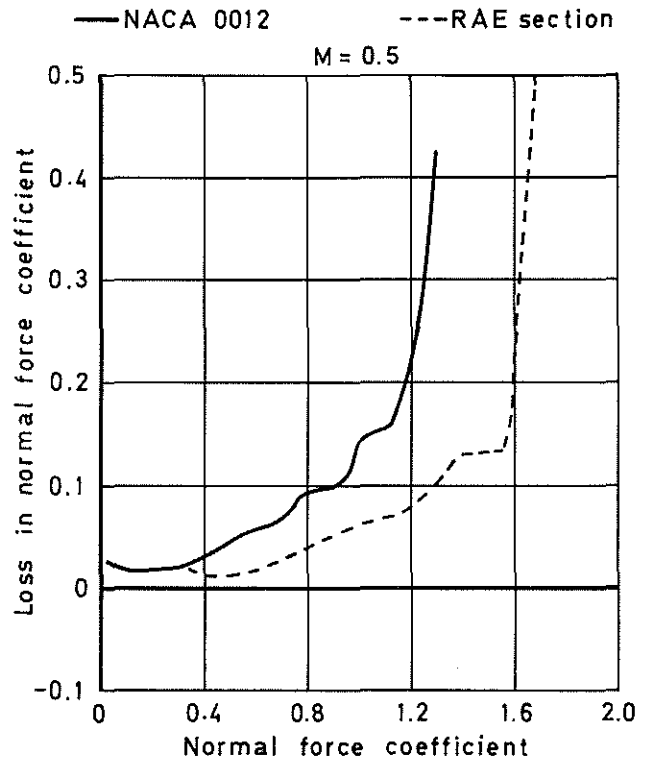


Fig 19 Loss of normal force coefficient for $x/c = 2\%$, $z/c = 0.2\%$, 1500 deg/s ramp

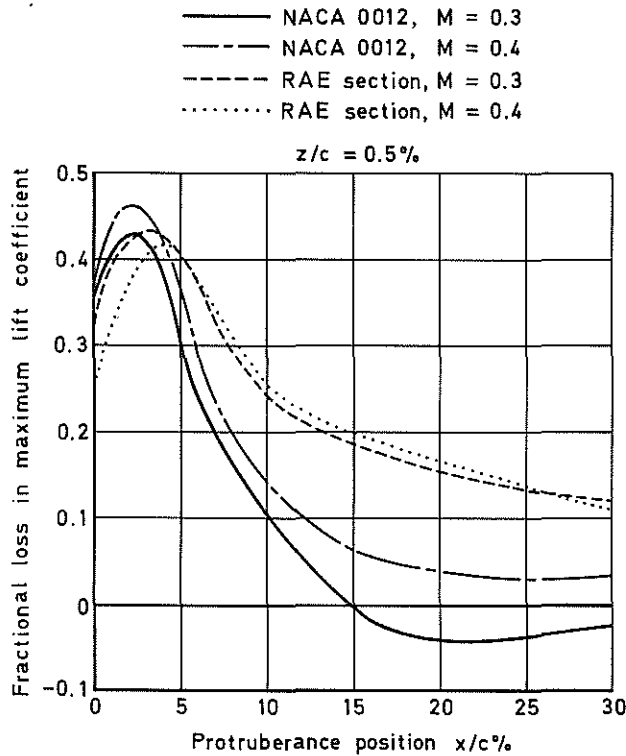


Fig 20 Fractional loss of maximum lift coefficient for quasi-steady motion

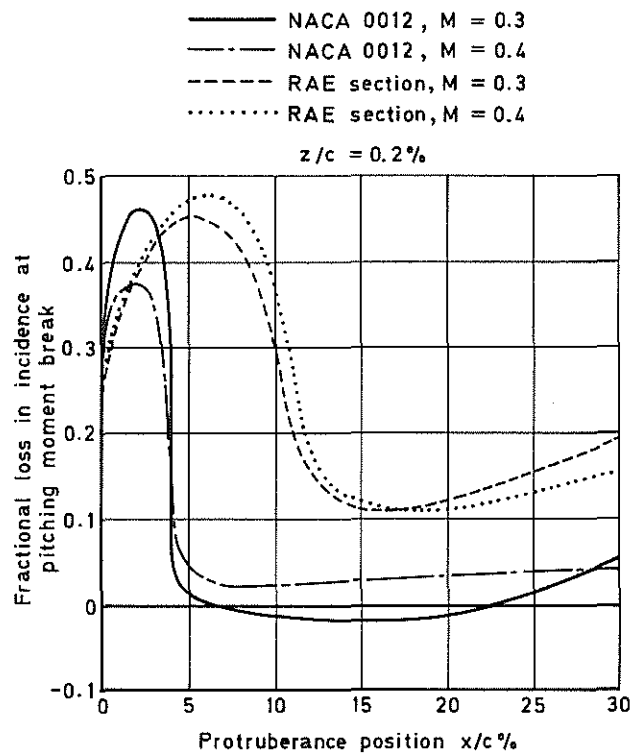


Fig 21 Fractional loss in incidence at pitching moment break for 1500 deg/s ramp